frontiers | Frontiers in Cellular and Infection Microbiology

TYPE Original Research
PUBLISHED 25 March 2024
DOI 10.3389/fcimb.2024.1363407



OPEN ACCESS

EDITED BY
Chen Zhao,
Fudan University, China

REVIEWED BY
Norberto Gonzalez-Juarbe,
J. Craig Venter Institute (La Jolla),
United States
Li Xing,
Shanxi University, China
Amie J. Eisfeld,
University of Wisconsin-Madison,
United States

*CORRESPONDENCE
Benjamin Koch
B.Koch@med.uni-frankfurt.de
Stephan Pleschka
stephan.pleschka@viro.med.uni-giessen.de

†These authors share last authorship

RECEIVED 30 December 2023
ACCEPTED 29 February 2024
PUBLISHED 25 March 2024

CITATION
Koch B, Shehata M, Müller-Ruttloff C, Gouda SA, Wetzstein N, Patyna S, Scholz A, Schmid T, Dietrich U, Münch C, Ziebuhr J, Geiger H, Martinez-Sobrido L, Baer PC, Mostafa A and Pleschka S (2024) Influenza A virus replicates productively in primary human kidney cells and induces factors and mechanisms related to regulated cell death and renal pathology observed in virus-infected patients.
*Front. Cell. Infect. Microbiol.* 14:1363407.
doi: 10.3389/fcimb.2024.1363407



# Influenza A virus replicates productively in primary human kidney cells and induces factors and mechanisms related to regulated cell death and renal pathology observed in virus-infected patients

Benjamin Koch[1*], Mahmoud Shehata[2,3], Christin Müller-Ruttloff[3,4], Shady A. Gouda[5], Nils Wetzstein[6], Sammy Patyna[1], Anica Scholz[7], Tobias Schmid[7], Ursula Dietrich[8], Christian Münch[5,9,10], John Ziebuhr[3,4], Helmut Geiger[1], Luis Martinez-Sobrido[11], Patrick C. Baer[1], Ahmed Mostafa[2,11†] and Stephan Pleschka[3,4*†]

[1]Department of Internal Medicine 4, Nephrology, University Hospital, Goethe University Frankfurt, Frankfurt am Main, Germany, [2]Center of Scientific Excellence for Influenza Viruses, National Research Centre (NRC), Cairo, Egypt, [3]Institute of Medical Virology, Justus Liebig University Giessen, Giessen, Germany, [4]German Center for Infection Research (DZIF), Partner Site Giessen, Giessen, Germany, [5]Institute for Biochemistry II, Goethe University Frankfurt, Frankfurt am Main, Germany, [6]Department of Internal Medicine 2, Infectious Diseases, Goethe University Frankfurt, Frankfurt am Main, Germany, [7]Institute of Biochemistry I, Goethe University Frankfurt, Frankfurt am Main, Germany, [8]Institute for Tumor Biology and Experimental Therapy, Georg-Speyer-Haus, Frankfurt am Main, Germany, [9]Frankfurt Cancer Institute (FCI), Frankfurt am Main, Germany, [10]Cardio-Pulmonary Institute, Frankfurt am Main, Germany, [11]Texas Biomedical Research Institute, Disease Intervention & Prevention (DIP) and Host Pathogen Interactions (HPI) Programs, San Antonio, TX, United States

**Introduction:** Influenza A virus (IAV) infection can cause the often-lethal acute respiratory distress syndrome (ARDS) of the lung. Concomitantly, acute kidney injury (AKI) is frequently noticed during IAV infection, correlating with an increased mortality. The aim of this study was to elucidate the interaction of IAV with human kidney cells and, thereby, to assess the mechanisms underlying IAV-mediated AKI.

**Methods:** To investigate IAV effects on nephron cells we performed infectivity assays with human IAV, as well as with human isolates of either low or highly pathogenic avian IAV. Also, transcriptome and proteome analysis of IAV-infected primary human distal tubular kidney cells (DTC) was performed. Furthermore, the DTC transcriptome was compared to existing transcriptomic data from IAV-infected lung and trachea cells.

**Results:** We demonstrate productive replication of all tested IAV strains on primary and immortalized nephron cells. Comparison of our transcriptome and proteome analysis of H1N1-type IAV-infected human primary distal tubular cells (DTC) with existing data from H1N1-type IAV-infected lung and primary trachea

10.3389/fcimb.2024.1363407

cells revealed enrichment of specific factors responsible for regulated cell death in primary DTC, which could be targeted by specific inhibitors.

**Discussion:** IAV not only infects, but also productively replicates on different human nephron cells. Importantly, multi-omics analysis revealed regulated cell death as potential contributing factor for the clinically observed kidney pathology in influenza.

KEYWORDS

**influenza A virus, acute kidney injury, distal tubular cells, transcriptomics, proteomics, regulated cell death**

## 1 Introduction

Influenza A viruses (IAV) have a single-stranded and segmented RNA genome of negative polarity ((−)ssRNA). In humans, IAV has a predominant tropism for epithelial cells in the respiratory tract (Ibricevic et al., 2006) and is responsible for seasonal local, epidemic, and pandemic outbreaks. Clinical manifestations of IAV infection can vary between aggravated common cold symptoms and severe complications, including a frequently lethal acute respiratory distress syndrome (ARDS). In the United States of America (USA), seasonal human influenza results in approximately 14.5 million medical visits annually (Matias et al., 2016), about 700,000 hospitalizations, and up to 80,000 influenza-related deaths (Rolfes et al., 2018). The influenza case fatality rate (CFR) is usually low (Taubenberger and Morens, 2006), but because of widespread infection, even seasonal influenza-associated respiratory deaths are estimated to account for more than 500,000 deaths per year globally (Iuliano et al., 2018). Infections of a largely immunologically naïve human population with antigenically new IAV variants were associated with an increased CFR. Thus, for example, in 1918, about 500 million people (one-third of the world human population at the time) were infected by an immunogenically new and more pathogenic H1N1 IAV, resulting in an estimated 50–100 million deaths (Johnson and Mueller, 2002; Morens and Taubenberger, 2018).

In humans, the clinical outcome of IAV infections is related to specific features of the viral genome, patient age, pre-existing comorbidities, viral load, and spread to the lower airways and lung, resulting in viral pneumonia (Siefkes et al., 2015). The particular importance of IAV-related respiratory failure (IAV-ARDS) is well known and mainly based on the infection and lysis of alveolar epithelial and endothelial cells, as well as the resulting inflammation, activation of macrophages, hypercytokinemia, and bacterial co- or superinfections (Short et al., 2014). In addition, extrapulmonary complications result in increased morbidity as well as mortality (Lee et al., 2011), and there is evidence to suggest a link to IAV viremia (Kaji et al., 1959; Zhadanov, 1960; Khakpour et al., 1969; Yawn et al., 1971; Jong et al., 2006; Tse et al., 2011).

Notably, human and avian IAV receptors are present in human kidney cells (Ulloa and Real, 2001; Yao et al., 2008), and—in addition to liver, spleen, heart, and muscle—infectious IAV has been isolated from kidney tissue in human autopsies (Kaji et al., 1959; Gamboa et al., 1979). Furthermore, IAV could be detected in the urine of patients during several pandemic outbreaks (Figure 1)

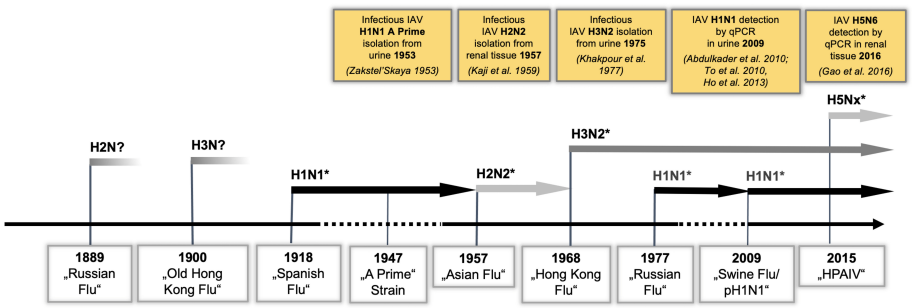


FIGURE 1
IAV strains detected in renal tissue reflect the dominant circulating strains. IAV pandemic outbreaks and currently cocirculating H1N1, H3N2, and H5Nx strains are indicated. PCR detection or isolation of infectious IAV from renal tissue/urine is illustrated in yellow boxes. (*PCR-confirmed IAV strains).

(Zakstel', 1953; Khakpour and Nik-Akhtar, 1977; Abdulkader et al., 2010; To et al., 2010; Ho et al., 2013). A recent meta-analysis showed that the rate of positive urine tests for IAV was 58% in patients infected with IAV (Lowry et al., 2023). Importantly, the 2009 pandemic was associated with significant extrapulmonary complications (Lee et al., 2011), among which IAV-induced acute kidney injury (IAV-AKI) was related to increased mortality (Abdulkader et al., 2010; Martin-Loeches et al., 2011; Nin et al., 2011a; Thakkar and Golestaneh, 2021), and this trend is continuing in IAV-AKI (Ersoy et al., 2021; Hsu et al., 2022; Jamoussi et al., 2022). Yet, the pathophysiology of IAV-AKI is incompletely understood (Joannidis and Forni, 2011; Watanabe, 2013). Intriguingly, in many lethal cases of human IAV infections, acute tubular necrosis (ATN) of distal tubular cells (DTC) (Beswick and Finlayson, 1959) and viral antigen in DTC and glomerular cells was demonstrated (Zinserling et al., 1983; Nin et al., 2011b). Therefore, the aim of the present study was to assess IAV replication in distinct cells of the kidney, to study alterations of the transcriptome and proteome responses of these cells after IAV infection with the goal of identifying signaling pathway alterations in IAV-AKI, and to compare them to those from IAV-infected lung and primary trachea cells.

# 2 Materials and methods

## 2.1 Cells

Proximal tubular cells (PTC) and DTC were isolated from human kidney tissue provided by Rita Schmitt-Prokopp and Michael Lein (Department of Urology, Sana Hospital, Offenbach, Germany) using magnetic cell separation technology as described previously (Baer et al., 1997). For the isolation of PTC, a monoclonal antibody (mAb) against aminopeptidase N/M (CD13, Cat. No. sc-18899, Santa Cruz, Dallas, Texas, USA, RRID : AB_626895) was used, specific for the proximal tubule. DTC was isolated using a mAb recognizing Tamm Horsfall glycoprotein (THG, clonotype No. 109, purified supernatant from hybridoma provided by Prof. Juergen Scherberich, Munich), a specific antigen of the thick ascending limb of Henle's loop and the early distal convoluted tubule. DTC was maintained in M199 medium (Sigma-Aldrich, Steinheim, Germany) supplemented with 10% fetal bovine serum (FBS, Biochrom, Berlin, Germany). Conditionally immortalized human glomerular endothelial (CiGEnC, RRID : CVCL_W185), human mesangial (K29-Mes, RRID : CVCL_W168), and human podocyte (Ly8 + 13, RRID : CVCL_W186) cell lines were kindly provided by Simon C. Satchell and Moin A. Saleem (both Bristol Renal, University of Bristol, UK) and maintained according to previously established cell culture protocols (Saleem et al., 2002; Satchell et al., 2006; Sarrab et al., 2011). Briefly, CiGEnC was cultured using EGM-2MV medium + Bullet Kit (No. CC-3202, Lonza, Walkersville, MD, USA). Until 90% confluence, cells were kept at 33°C to allow proliferation. Thereafter, the temperature was switched to 37°C for 10 days to initiate differentiation (all conditions in a 5% $CO_2$ atmosphere). K29-Mes and Ly8 + 13 cells were grown at 33°C with RPMI-1640 (ThermoFisher, Germany), 10% FBS, and insulin–transferrin–selenium (ITS, Sigma, No. 1884, final concentration (fconc.) $I$ = 5 µg/ml; $T$ = 5 µg/ml; $S$ = 5ng/ml). After reaching confluence (~80%–90%), they were differentiated at 37°C for 14 days (all conditions in a 5% $CO_2$ atmosphere). Madin–Darby canine kidney cells II (MDCK.2, RRID : CVCL_0424) were acquired originally from ATCC and were passaged in DMEM (ThermoFisher, Germany) supplemented with 5%–10% FBS, 100 IU penicillin, and 100 µg streptomycin (P/S)/ml at 37°C in a 5% $CO_2$ atmosphere.

## 2.2 Viruses

Human influenza viruses A/Giessen/6/09 H1N1 ($H1N1_{pdm09}$) (Mostafa et al., 2013) and A/Victoria/3/75 H3N2 ($H3N2_{Victoria}$) were obtained from the virus collection of the Institute of Medical Virology, Justus Liebig University Giessen, Germany. The human isolates of a highly pathogenic avian influenza virus (HPAIV), A/Egypt/MOH-NRC-7305/2014 H5N1 ($H5N1_{MOH\text{-}NRC}$), and A/Anhui/1/2013 H7N9 ($H7N9_{Anhui/1}$) were kindly provided by M.A. Ali (National Research Center, Cairo, Egypt) and T. Wolff (Robert Koch-Institute, Berlin, Germany), respectively. Stocks of $H1N1_{pdm09}$, $H3N2_{Victoria}$, $H5N1_{MOH\text{-}NRC}$, and $H7N9_{Anhui/1}$ were generated on MDCK-II monolayers in the presence of TPCK-treated trypsin as previously described (Pleschka et al., 2016). Briefly, virus stocks were prepared as clarified cell-free supernatants by centrifugation at 800×$g$ for 5 min, aliquoted, and stored at −80°C.

To achieve a sufficiently high $H1N1_{pdm09}$ concentration for omics experiments, one-half of the clarified cell-free supernatant of the $H1N1_{pdm09}$ virus was further concentrated by ultracentrifugation as previously described (Pleschka et al., 2016). Briefly, virus particles in the cell-free supernatant of $H1N1_{pdm09}$ were pelleted through a sucrose cushion. A volume of 30 ml of the virus preparation was carefully pipetted on top of a 20% sucrose solution (12 ml) and then centrifuged using a Beckman SW28 rotor at 28,000 r.p.m. for 2 h at 4°C. The pellet was resuspended in 500 µl of PBS. A virus titer of $6 \times 10^7$ focus-forming units (FFU)/ml was determined by focus formation assay, and the preparation was stored at −80°C.

## 2.3 Focus formation assay

Virus titers were determined using a focus formation assay as described earlier (Ma et al., 2009). Briefly, 90% confluent MDCK-II cells grown in 96-well plates were washed with PBS++ (PBS containing 1 mM $MgCl_2$ and 0.9 mM $CaCl_2$). Subsequently, 50 µl of virus-containing supernatant in a 10-fold dilution in PBS/BSA/P/S (PBS++ containing 0.2% BSA; P/S) was added. After 1 h of viral adsorption at room temperature (rt), the virus inoculum was replaced by 150 µl of titration medium (10% of 10× MEM, 33% $ddH_2O$, P/S, 1% of 30% BSA, 50% of 1.25% Avicel (DuPont Nutrition Biosciences, Braband, Denmark), 1% DEAE-Dextran, 4% of 7.5% $NaHCO_3$, and 2 µg/ml of TPCK-treated trypsin (all tested IAV strains require TPCK-treated trypsin except

$H5N1_{MOH\text{-}NRC}$). After 24 h postinfection (hpi) at 37°C, the cells were fixed and permeabilized with 330 µl fixing solution (PBS++ containing 4% paraformaldehyde (PFA) and 1% Triton X-100), stored at 4°C for 60 min followed by three washes with PBS/Tween (PBS containing 0.05% Tween 20) and were then incubated for 1 h at rt with 50 µl of first antibody (mouse anti-influenza A nucleoprotein mAb, hybridoma supernatant provided by Prof. Stephan Ludwig, University Muenster, Germany) diluted 1:100 in PBS/BSA (PBS containing 3% BSA). Cells were then washed three times with PBS/Tween and incubated with a second antibody (antimouse HRP antibody, SantaCruz sc2005, RRID : AB_631736) diluted 1:100 in PBS/BSA at rt for 60 min. To detect foci, the washed cells were incubated with 40 µl/well of AEC staining solution (Sigma-Aldrich, USA). For analysis, the 96-well plates were scanned and analyzed using the Photoshop software package (Adobe Systems, San Jose, CA, USA). All titrations were performed in duplicate.

## 2.4 Growth kinetics

PTC, DTC, CiGEnC, CiMes, and CiPod were plated in six-well plates at a density of $4 \times 10^5$ cells per well for the infection experiments. Infections with $H1N1_{pdm09}$, $H3N2_{Victoria}$, $H5N1_{MOH\text{-}NRC}$, and $H7N9_{Anhui/1}$ were carried out in triplicates at a multiplicity of infection (MOI) of 0.1 and incubated at 37°C in the appropriate medium containing TPCK-treated trypsin (except for $H5N1_{MOH\text{-}NRC}$). Cell culture supernatants from infected and control animals were harvested at 12 hpi, 24 hpi, 36 hpi, and 48 hpi. The virus titers were determined by focus formation assay (FFU/ml) using MDCK-II cells.

## 2.5 Infections and sample collection

PTC, DTC, CiGEnC, CiMes, and CiPod were plated in six-well plates at a density of $4 \times 10^5$ cells per well. Infections for OMIC analysis were carried out with $H1N1_{pdm09}$ (MOI = 1). For gene expression analysis, infected DTC were collected in RLT+β-mercaptoethanol lysis buffer (Qiagen, Hilden, Germany) at the indicated time points hpi. For mass spectrometry, DTC monolayers were washed twice with PBS++, scratched off, and collected in 1 ml of PBS. The cells were then pelleted by centrifugation for 30 s at 13,000×*g* at 4°C. The supernatant was discarded, and cell pellets were lysed on ice for 10 min using lysis buffer (TLB: 25 mM Tris, pH 8.0; 137 mM NaCl; 10% glycerol; 0.1% sodium dodecyl sulfate; 0.5% sodium deoxycholate; 1% NP-40; 2 mM EDTA, pH 8.0; 0.2 mM pefablock; 5 µg/ml aprotinin; 5 µg/ml leupeptin; 1 mM Na-vanadate; and 5 mM benzamidine). Subsequently, the samples were centrifuged at 13,000×*g* at 4°C for 30 min, and the supernatants were collected for subsequent analyses.

## 2.6 RT-qPCR analysis

Relative expression levels of selected mRNAs were quantified following infection with DTC (MOI = 1). Total RNA was extracted using the RNeasy Maxi Kit (Qiagen, Hilden, Germany), including on-column removal of DNA by digestion with rDNase for 15 min at rt, and cDNA for quantitative real-time RT-PCR (qPCR) was synthesized using 1,000 ng RNA in a 15-µl reaction volume. qPCR reactions were set up to a final volume of 20 µl using the HOT FIREPol® EvaGreen® qPCR Supermix (Solis Biodyne, Tartu, Estonia) and primers for ß-ACTIN (FWD 5′-ACTGGAACGGTGAAGGGTGAC-3′, REV 5′-AGAGAAGTGGGGTGGCTTTT-3′, product size: 169 bp), MLKL (FWD 5′-AAGAAGGTGGAAGAGCGAGC-3′, REV 5′-TCCTTGGTCCTGGAGCATCT-3′, product size: 186 bp), and ZBP1 (FWD 5′-ACCTTCTGGACATGGATGAGCA-3′, REV 5′-AGGCTGACTTTGCTCTTCTTCC-3′, product size: 81 bp). The qPCR reaction was run on an ABI PRISM 7900HT Fast Real-Time PCR System with Sequence Detection System SDS 2.4.1 software (both Applied Biosystems, Waltham, MA, USA), using 40 cycles of the following program: 95°C for 15 s, 63°C for 15 s, and 72°C for 20 s (SDS 2.4.1. settings: automatic baseline, threshold 0.2). To exclude artifacts resulting from primer dimer formation, melting curve analysis was performed using the sequence 95°C for 15 s, 60°C for 15 s, 95°C for 1 min, and 37°C for 30 s. The results shown represent the mean of three independent experiments. Relative expression of the mRNA target was assessed using the ΔΔCt method (Pfaffl, 2001), with β-actin as calibrator, and levels of target gene expression were estimated by $2^{-\Delta\Delta Ct}$. Statistical significance was determined by GraphPad Prism software version 9.0 for OS X (GraphPad Software Inc., La Jolla, CA, USA) with a two-way ANOVA and *t*-test.

## 2.7 Transcriptome analysis

Six biological replicates of DTC grown in six-well plates were either left uninfected or infected with $H1N1_{pdm09}$ at a MOI = 1. Two replicates of each set were analyzed for transcript expression changes by RNAseq, while the remaining replicates were used for verification of RNAseq results by qPCR (RT-qPCR for ZBP1 and MLKL, Supplementary Figure S1). Briefly, total RNA was extracted 12 hpi of the $H1N1_{pdm09}$-infected/noninfected DTC by Qiagen RNeasy Maxi Kit (Qiagen, Germany), including on-column removal of DNA by digestion with rDNase for 15 min at rt. For library preparation, 500 ng of RNA (each showing a RIN score from > 9) was used. Second to depletion of ribosomal RNA (QIAseq FastSelect RNA Removal Kit, Qiagen, Germany), directional libraries were prepared with a NEBNext® UltraTM Directional RNA Library Prep Kit for Illumina® sequencing (No. E7420S, New England Biolabs, Ipswich, MA, USA). Sequencing was performed by an Illumina NextSeq500® using a NextSeq® 500/550 High Output Kit v2 (75 cycles, No. FC-404-2005, Illumina, San Diego, CA, USA). Illumina BCL files were converted to FASTQ by bcl-convert (Illumina, San Diego, CA, USA), quality controlled by FastQC (Babraham Institute, Cambridge, UK, http://www.bioinformatics.babraham.ac.uk/projects/fastqc/) and Illumina adapters trimmed by Trimmomatic v0.40 (Bolger et al., 2014). Quantification of transcript expression was performed by "kallisto" software (Bray et al., 2016) (version 0.46.1) with standard configurations using a kallisto index build from the hg38 assembly (GRCh38.p12 cDNA). "sleuth" (Pimentel et al., 2017) software (version 0.30.0) was used for differential expression analysis with the Wald test setting for comparison of the two groups. Raw

(FASTQ), kallisto, and sleuth data are available from NCBI Gene Expression Omnibus (GEO), https://www.ncbi.nlm.nih.gov/geo/query/acc.cgi?acc=GSE189735. DTC transcriptome data were supplemented by existing GEO datasets of IAV-infected cells. The FASTQ datasets (GSE103604, GSE89008) from $H1N1_{A/PR/8/1934}$-infected adenocarcinomic human alveolar basal epithelial (A549) cells (Zhao et al., 2018) as well as from $H1N1_{A/California/04/09}$-infected human bronchial tracheal epithelial (HBTE) cells (Heinz et al., 2018), compared to mock control at 12 hpi, were reanalyzed by kallisto and sleuth software in order to create a homogenous basis for the comparison with the data gained from the $H1N1_{pdm09}$-infected DTCs. All results were investigated for pathway over-representation at the gene level (cut off: at least 2 genes in pathway annotation and $p < 0.01$) by ConsensusPathDB (Kamburov et al., 2011) (http://cpdb.molgen.mpg.de/, Release 35, database = 05.06.2021) employing "Kyoto Encyclopedia of Genes and Genomes (KEGG)" (Kanehisa, 2000), Reactome (Vastrik et al., 2007), and Wikipathways (Pico et al., 2008). GO analysis was performed by ShinyGO v0.77 (Ge et al., 2019). MA plots, heatmaps, and KEGG enrichment/mapping were done by the "R package iDEP" (version 1.0) and "pathview" software (version 1.38) (Luo and Brouwer, 2013; Ge et al., 2018). Network analysis of differentially regulated coding genes using the Ensembl gene set ("ENSG") was performed by "STRING v11.0" (Mering et al., 2003) software (https://string-db.org) using standard parameters. Next, the network was imported into "Cytoscape 3.8.0" software (https://cytoscape.org) (Shannon et al., 2003), and centrality analysis (top 10 nodes ranked by degree scores) was performed using the "Cytoscape plugin CytoHubba v0.1" (Chin et al., 2014). For Venn (overlap) analysis, BioTools.fr (http://biotools.fr/misc/venny) was utilized.

## 2.8 Sample preparation for LC-MS

Lysates were precipitated using volumes of ice-cold methanol/chloroform/dd$H_2O$ (3:1:2.5). After centrifugation at 14,000×*g* for 45 min at 4°C, the upper aqueous phase was aspirated, and 3 volumes of ice-cold methanol was added. Samples were mixed, and proteins were pelleted by centrifugation at 14,000×*g* for 5 min at 4°C. The supernatant was discarded, and the pellets were washed one additional time with ice-cold methanol. Protein pellets were dried at rt for further use. Proteins were resuspended in 8 M urea, 10 mM EPPS at pH 8.2, and 1 mM $CaCl_2$, and protein concentration was determined using a BCA assay (No. 23235, ThermoFisher Scientific, Waltham, MA, USA). Samples were then diluted to 2 M urea using digestion buffer (10 mM EPPS at pH 8.2, 1 mM $CaCl_2$) and incubated with LysC (Wako Chemicals, Osaka, Japan) at a 1:50 (w/w) ratio overnight at 37°C. The next day, digestion reactions were further diluted to 1 M urea using digestion buffer and incubated at a 1:100 (w/w) ratio of trypsin (No. V5113, Promega, Madison, WI, USA) for an additional 6 h at 37°C. Digests were acidified using trifluoroacetic acid (TFA) to a pH of 2–3, and peptides were purified using Sep-Pak C18 columns (No. WAT054955, Waters, Milford, MA, USA) according to the manufacturer's protocol. The eluates were dried and stored for further processing. Peptides were resuspended in TMT-labeling buffer (0.2 M EPPS at pH 8.2, 10% acetonitrile), and peptide concentration was determined by BCA assay. Peptides were mixed with TMT reagents (No. 90111, No. A37724, No. 90061, ThermoFisher Scientific, USA) in a 1:2 (w/w) ratio (2 mg TMT reagent per 1 mg peptide). Reactions were incubated for 1 h at rt and subsequently quenched by the addition of hydroxylamine to a final concentration of 0.5% at rt for 15 min. Samples were pooled in equimolar ratio, acidified, and dried for further processing. Before MS analysis, peptide samples were purified using Empore C18 (Octadecyl) resin material (3 M Empore, St. Paul, MN, USA). The material was activated by incubation with methanol for 5 min, followed by one wash each with 70% acetonitrile/0.1% TFA and 5% acetonitrile/0.1% TFA. Samples were resuspended in 5% acetonitrile/0.1% TFA and loaded onto the resin material. Peptides were washed with 5% acetonitrile/0.1% TFA and eluted with 70% acetonitrile (ACN). Samples were dried and resuspended in 0.1% formic acid (FA) for LC-MS2/3.

## 2.9 High-pH reverse phase fractionation

Peptides were either fractionated using a Dionex Ultimate 3000 analytical HPLC or a high-pH reversed-phase fractionation kit (ThermoFisher Scientific, USA). The latter was used according to the manufacturer's instructions. For high pH reversed-phase fractionation on the Dionex HPLC, 500 mg of pooled and purified TMT-labeled samples were resuspended in 10 mM ammonium bicarbonate (ABC), 5% ACN, and separated on a 250-mm-long C18 column (Aeris Peptide XB-C18, 4.6 mm ID, 2.6 mm particle size; Phenomenex, Torrance, CA, USA) using a multistep gradient from 100% solvent A (5% ACN, 10 mM ABC in water) to 60% solvent B (90% ACN, 10 mM ABC in water) over 70 min. Eluting peptides were collected every 45 s into fractions, which were cross-concatenated and dried for further processing.

## 2.10 Mass spectrometry

Peptides were resuspended in 0.1% FA and separated on an Easy nLC 1200 (ThermoFisher Scientific, USA) and a 22-cm-long, 75-mm ID fused-silica column, which had been packed in-house with 1.9 mm C18 particles (ReproSil-Pur, Dr. Maisch, Germany), and kept at 45°C using an integrated column oven (Sonation, Biberach, Germany). Peptides were eluted by a nonlinear gradient from 5% to 38% acetonitrile over 120 min and directly sprayed into a QExactive HF mass spectrometer equipped with a nanoFlex ion source (ThermoFisher Scientific, USA) at a spray voltage of 2.3 kV. Full-scan MS spectra (350–1,400 m/z) were acquired at a resolution of 120,000 at m/z 200, a maximum injection time of 100 ms, and an AGC target value of 33,106. Up to 20 most intense peptides per full scan were isolated using a 1-Th window and fragmented using higher-energy collisional dissociation (normalized collision energy of 35). MS/MS spectra were acquired with a resolution of 45,000 at m/z 200, a maximum injection time of 80 ms, and an AGC target value of 13,105. Ions with charge states of 1 and > 6, as well as ions with unassigned charge states, were not considered for fragmentation. Dynamic exclusion was set to 20 s to minimize repeated sequencing of already-acquired precursors.

## 2.11 Processing of proteomics raw files and data analysis

Raw files were analyzed using Proteome Discoverer (PD) 2.2 software (ThermoFisher Scientific, USA). Files were recalibrated using the Homo sapiens SwissProt database (TaxID:9606, version 2017-06-07). Spectra were selected using default settings, and database searches were performed using the SequestHT node in PD. Database searches were performed against trypsin-digested Homo sapiens SwissProt database and FASTA files of common contaminants ("contaminants.fasta" provided with MaxQuant) for quality control. The results were then exported to Excel files for further processing. Log2 fold changes were calculated by log2 transformation of the ratio between the mean of the replicates of treated samples versus the control samples. Significance was assessed by unpaired, two-sided Student's *t*-test. *p*-values were adjusted by a Benjamini–Hochberg FDR correction. Adjusted *p*-values (*q*-values) lower than 0.05 were considered significant. *n* represents the number of independent replicates. Data are available via https://www.ebi.ac.uk/pride/archive with identifier PXD030093.

## 2.12 Cell viability and viral inhibition assays

Confluent layers of DTC in 96-well plates were infected with $H1N1_{pdm09}$ or $H3N2_{Victoria}$ at a MOI of 0.1. One hour after infection, emricasan (EM, No. HY-10396, MedChemExpress, Monmouth Junction, NJ, USA) and necrosulfonamide (NSA, No. HY-100573, MedChemExpress, USA) were added at different concentrations (EM: 10 μM, NSA: 5 μM, or EM: 10 μM + NSA 5 μM) and cells incubated at 37°C for 24 hpi in M199 (containing 0.2% bovine serum albumin (BSA) (Sigma, Germany) and 1 μg/ml of TPCK-treated trypsin. Cytopathogenic effects/viability was assessed using CellTox™ Green Cytotoxicity Assay (No. G8741, Promega, USA) and RealTime-Glo™ Extracellular ATP Assay (No. GA5010, Promega, USA). Data for each condition were collected for at least three biological replicates using a Spark 10M multimode microplate reader (Tecan, Zurich, Switzerland). Epithelial protection was calculated as a relative reduction of viability loss compared to uninfected controls. The cytotoxicity of the different inhibitors was determined using the tetrazolium derivate XTT (XTT Cell Viability Kit, Biotium, Hayward, CA, USA) according to the manufacturer's protocol. Briefly, DTC was seeded in 96-well plates and incubated for 24 h with the agent to be tested at the indicated final concentrations. Next, activated XTT was added, and after 5 h of incubation at 37°C, the absorbance was measured by a microplate reader (LB 911 Apollo-1, Berthold Technologies, Bad Wildbad, Germany) at 450 nm.

## 2.13 Quantification and statistical analysis

Results were expressed as the mean ± standard deviation (SD). Error bars represent the mean ± SD of at least three independent experiments. The difference between the two mean values was analyzed using Dunnett's multiple comparison test or Student's *t*-test using GraphPad Prism software version 9.0 for OS X (GraphPad Software Inc., USA). The difference was considered statistically significant when $p < 0.05$. Constitutive gene expression was assumed within a log2 fold change (log2FC) of ± 0.25.

## 2.14 Biosafety

All experiments with infectious viruses were performed according to German regulations for the propagation of IAV. All experiments involving HPAIV were performed in a biosafety level 3 (BSL3) containment laboratory approved for such use by the local authorities (RP, Giessen, Germany).

## 2.15 Ethics approval statement

The authors have no ethical conflicts to disclose. The procurement procedure for human PTC and DTC isolation was approved by the ethics committee of the Goethe-University Hospital Frankfurt, Germany, file number UGO 03/10–4/09.

# 3 Results

## 3.1 Human and avian IAV can infect and replicate in human kidney cells *in vitro*

To investigate whether IAV can infect and replicate productively in human kidney cells, primary proximal (PTC) and distal tubular cells (DTC), as well as immortalized glomerular endothelial (CiGEnC), mesangial (K29-Mes), and podocyte (Ly8 + 13) human cell lines, were used as an *in vitro* model. Cells were infected with $H1N1_{pdm09}$ and IAV $H3N2_{Victoria}$ human IAVs, as well as with human isolates of either low-pathogenic avian influenza virus (LPAIV) $H7N9_{Anhui/1}$ or highly pathogenic avian influenza virus (HPAIV) $H5N1_{MOH\text{-}NRC}$. The analysis of IAV titers in supernatants collected from these infected cells revealed remarkable differences in replication efficiency depending on the cell type and IAV strain used (Figure 2). Generally, primary tubular cells (DTC, PTC, Figure 2A) allowed replication of all IAV strains (Figures 2B, C). However, $H5N1_{MOH\text{-}NRC}$ and $H1N1_{pdm09}$ did not replicate in glomerular endothelial cells (CiGEnC, Figure 2D), and $H1N1_{pdm09}$ also did not replicate in mesangial cells (K29-Mes, Figure 2E) within 36 hpi and only late and with low titers on the podocyte cell line (Ly8 + 13, Figure 2F). In contrast to other IAV isolates, $H3N2_{Victoria}$ and $H7N9_{Anhui/1}$ replicated well on all cell types included in this analysis (Figures 2B–F). In conclusion, all investigated IAV strains replicated well on primary tubular cells. Given the *in vitro* data, it is possible that the different IAV strains may have different effects on renal pathology *in vivo*.

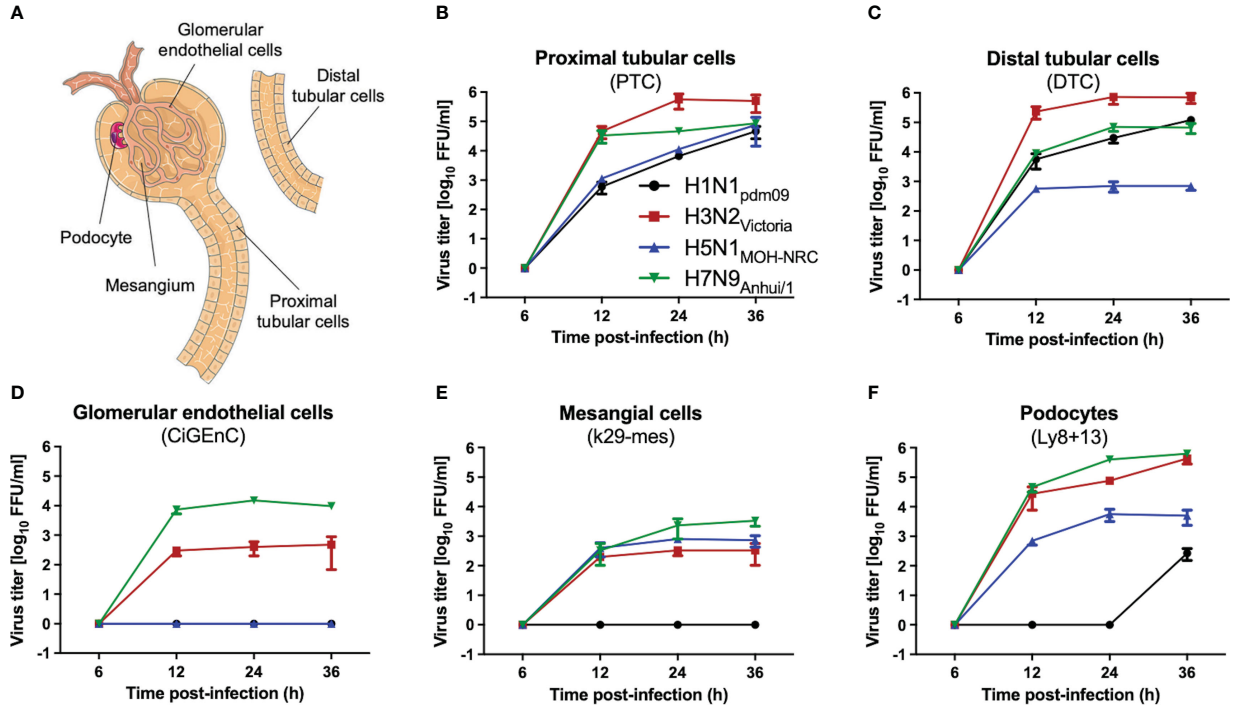


FIGURE 2
IAV replication on human kidney cells. Human primary (PTC, DTC) or immortalized (K29-Mes, CiGEnC, Ly8 + 13) kidney cells were infected with IAV $H1N1_{pdm09}$, $H3N2_{Victoria}$, $H5N1_{MOH-NRC}$, and $H7N9_{Anhui/1}$, and viral titers were determined by focus-forming assay (FFU/ml) at the indicated time points (error bars indicate standard deviations (SD) of the data obtained from three biological replicates at each time point). **(A)** A renal functional unit (nephron), loop of Henle omitted. **(B)** Human primary proximal tubular cells (PTC). **(C)** Human primary distal tubular cells (DTC). **(D)** Human conditionally immortalized glomerular endothelial cells (CiGEnC). **(E)** Human conditionally immortalized mesangial cells (K29-Mes). **(F)** Human conditionally immortalized podocytes (Ly8 + 13).

## 3.2 Transcriptome and proteome analysis of $H1N1_{pdm09}$-infected DTC

Based on these initial findings and because of the dominant DTC pathology observed in autopsies of H1N1-infected patients (Kuskow, 1895; Winternitz et al., 1920; Beswick and Finlayson, 1959; Zinserling et al., 1983; Nin et al., 2011a), we subsequently infected DTC for further mechanistical analyses. As IAV infection results in the specific inhibition of cellular mRNA processing and translation ("host-cell shut-off") (Bercovich-Kinori et al., 2016; Levene and Gaglia, 2018), analyses of both the transcriptome and proteome were performed at 12 hpi (Supplementary Tables S1, S2). Inoculation of DTC with $H1N1_{pdm09}$ resulted in highly significant transcriptional fold changes (Figures 3C, D) and protein abundances (Figures 4C, D) as compared to mock-infected DTC. To identify networks between cellular proteins, we employed STRING-DB network analysis. As this is based on protein/protein interactions, noncoding transcripts were excluded, and we restricted this analysis to those affected 1,753 protein-coding transcripts.

### 3.2.1 Transcriptome and proteome analysis of upregulated genes in $H1N1_{pdm09}$-infected DTC reveals a strong antiviral defense response

Among these 1,753 protein-coding transcripts, the top upregulated ones (Supplementary Table S1) are dominantly coding for interferon-induced proteins, like the antiviral-acting IFIT2, the double-stranded RNA sensor IFIH1, the inhibitors of viral endosomal fusion NCOA7 (219 aa isoform) and IFITM3, as well as the viral restriction factor MX1. Network analysis of upregulated protein-encoding transcripts in IAV-infected DTC (699) indicated 587 nodes (Figure 3A), of which the top 10 nodes (identified by centrality analysis) all include significantly upregulated transcripts coding for interacting factors involved in antiviral defense (Figure 3B). KEGG pathway analysis of differentially regulated genes (Figure 3D; Supplementary Table S3) highlighted factors known to be enriched in several viral infections—including IAV, as well as NOD-like- and RIG-I-like receptor signaling pathways, necroptosis, and the JAK-STAT signaling pathway (Figure 3E). Furthermore, KEGG mapping of upregulated transcripts in IAV-infected DTC highlighted most factors within the known KEGG-pattern of IAV infection (Supplementary Figure S2). In conclusion, transcriptome analysis emphasized the activation of IAV infection-specific KEGG-patterns, a strong induction of anti-viral defense, and necroptosis on the transcript level in IAV-infected DTC. As IAV infection results in "host-cell shut-off", we also analyzed the proteome of $H1N1_{pdm09}$-infected DTC at 12 hpi (Figure 4). Interestingly, as with the transcriptome, the proteomic network analysis—based on known interactions/functions and KEGG pathway analysis (Figure 4E) of differentially regulated proteins (Figures 4C, D)—also demonstrated that the upregulated proteins with the highest fold-change (Supplementary Table S2) were related to antiviral defense. Among these proteins are RSAD2, IFIT1, IFIT2, IFIT3, OASL, DDX60L,

10.3389/fcimb.2024.1363407

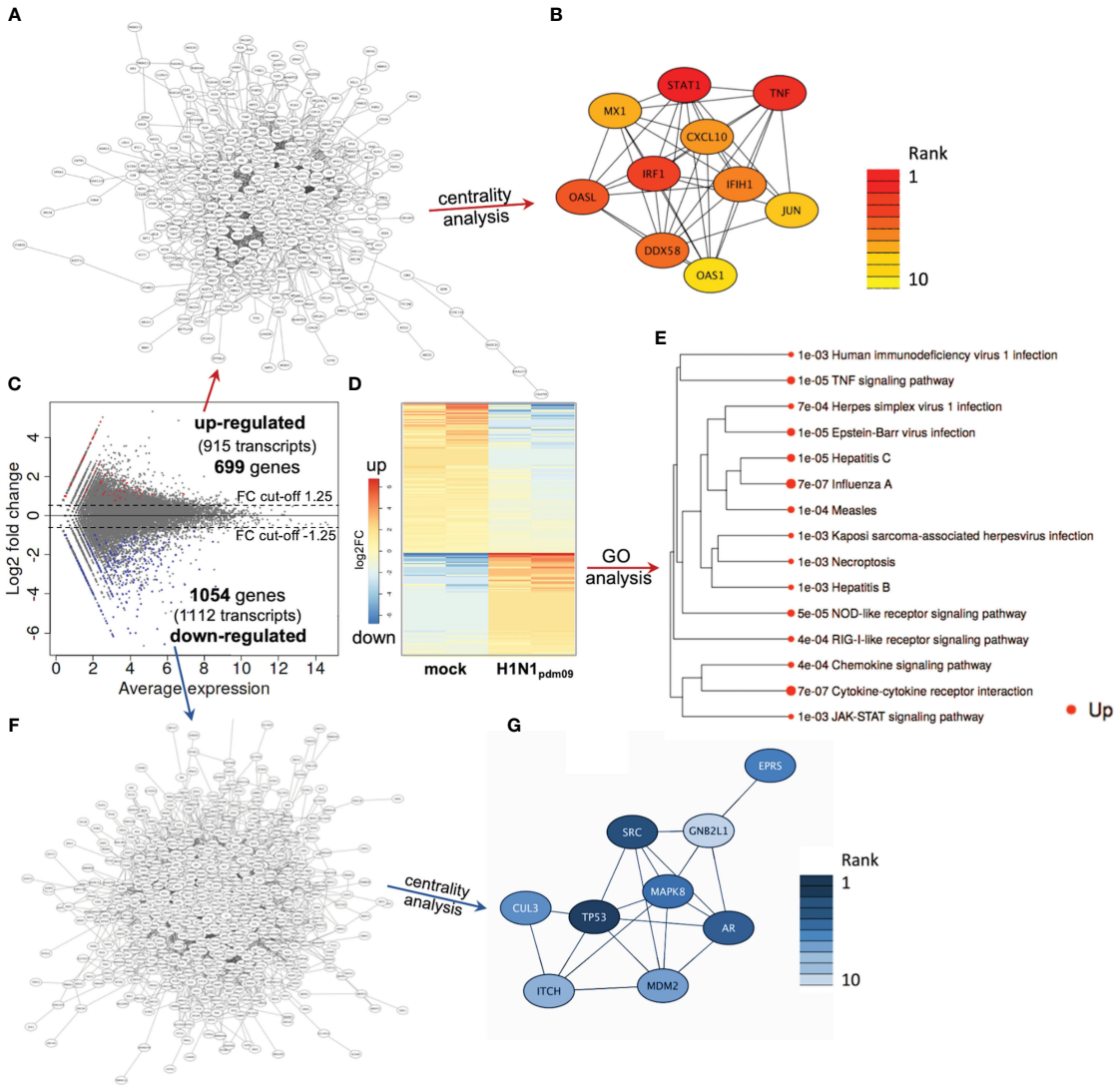


FIGURE 3
DTC transcriptomics. **(A)** Network of upregulated coding transcripts (587 nodes). **(B)** Network/centrality analysis for top 10 node interactions of proteins coded by upregulated transcripts (colored/dark red represents the highest centrality score). **(C)** MA plot of transcript expression changes 12 h after infection of DTC with $H1N1_{pdm09}$, showing significant changes in red (upregulated) and blue (downregulated). **(D)** Heatmap of differentially expressed genes ($H1N1_{pdm09}$-infected DTC vs. mock DTC, blue = downregulated, red = upregulated). **(E)** Enrichment tree of differentially regulated KEGG pathways from Figure 3D. The dot size represents the *q*-value (low *q*-value = large dot). **(F)** Network of downregulated coding transcripts (969 nodes). **(G)** Network/centrality analysis restricted to top 10 node interactions of proteins coded by downregulated transcripts (colored/dark blue represents the highest centrality score).

ISG20, and IRF9 (emphasized by centrality analysis, Figure 4B), as well as the MAP kinase MAP3K11 and the ubiquitin ligase HERC6. Taken together, interrogation of both upregulated transcriptome and proteome reveals a strong antiviral defense response in IAV-infected DTC (Figures 3A–E, 4A–E; Supplementary Tables S1–S3).

### 3.2.2 Transcriptome and proteome analysis of downregulated genes in $H1N1_{pdm09}$-infected DTC highlights factors regulated to translation, p53, and TGF-ß signaling

Next, the downregulated transcripts and proteins of IAV-infected DTC were investigated. Among the downregulated protein-coding transcripts, the p53 regulator MDM4, the central player in translation initiation EIF4G3, and the cytokine storm and mortality-associated Poly(rC)-binding protein 2 (PCBP2), known to be targeted by the H5N1 IAV-encoded miR-HA-3p (Li et al., 2018), were found within the top downregulated factors (Supplementary Table S1). Additionally, cell proliferation, androgen receptor (AR)-mediated signaling, and ubiquitination were pointed out by network analysis (Figures 3F, G). Pathway analysis of downregulated transcripts highlighted signaling by Rho GTPases, NRF2-ARE regulation, and Wnt signaling/pluripotency among the most significantly over-represented pathways (Supplementary Table S3). Taken together, transcripts of genes related to inhibitors of cytokine production and inflammation, as well as Rho GTPases, NRF2-ARE regulation, and Wnt signaling/pluripotency are predominant among downregulated transcripts in IAV-infected DTC (based on differential gene expression and

10.3389/fcimb.2024.1363407

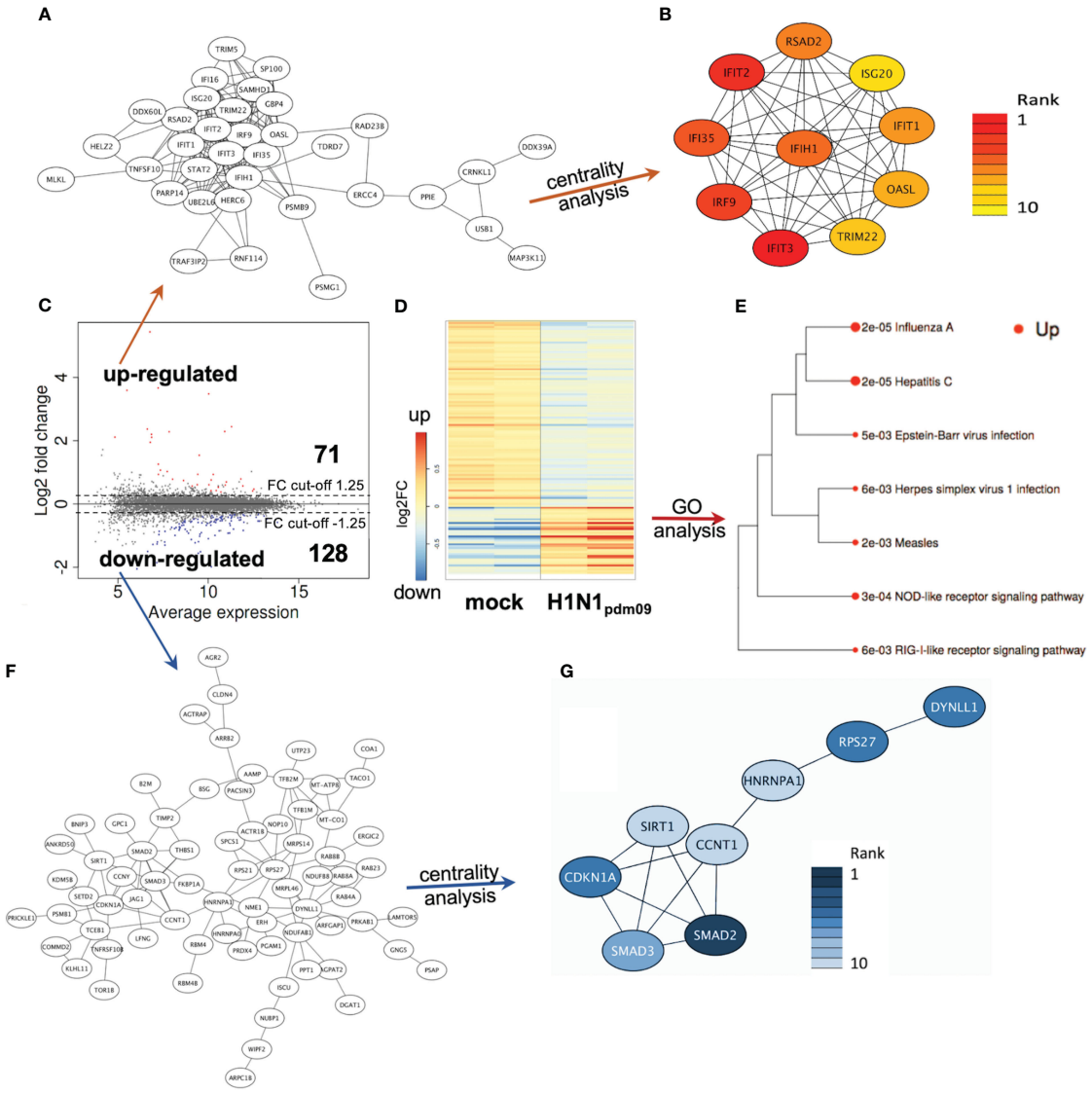


FIGURE 4
DTC proteomics. **(A)** Network of upregulated proteins (41 nodes). **(B)** Network/centrality analysis for top 10 node interactions of proteins (colored/dark red represents the highest centrality score). **(C)** MA plot of protein changes 12 h after infection of DTC with $H1N1_{pdm09}$, showing significant changes in red (upregulated) and blue (downregulated). **(D)** Heatmap of differentially regulated proteins in $H1N1_{pdm09}$-infected DTC vs. mock DTC (blue = downregulated, red = upregulated). **(E)** Enrichment tree of differentially regulated KEGG pathways from Figure 5D. The dot size represents the *q*-value (low *q*-value = large dot). **(F)** Network of downregulated proteins (84 nodes). **(G)** Network/centrality analysis restricted for the top 10 node interactions of downregulated proteins (colored/dark blue represents the highest centrality score).

pathway analysis). Compared to the number of upregulated proteins (71), the number of downregulated proteins with significant changes was almost double (128), which might be due to the IAV-induced "host-cell shutoff" and/or virus-induced repression of certain factors regulating transcription. Importantly, antiviral-acting proteins like the p53-interacting NME1 (Feng et al., 2018) as well as RPS27 (Li, 2019) were found among the most strongly downregulated proteins (Supplementary Table S2). Network analysis (top 10 nodes) underlined IAV-induced negative effects on transcription, translation, SMAD/TGF-ß signaling, cell cycle, intracellular transport, and alternative splicing (Figure 4G). Pathway analysis of all downregulated proteins included TGF-beta receptor signaling, endocytosis, FoxO signaling, and energy metabolism (Supplementary Table S3). Overall, the analysis of the top downregulated protein-encoding transcripts and expressed proteins revealed strong repression of cellular gene expression regarding antiviral acting proteins, the TP53 network, TGF-ß signaling, ubiquitination, transcription, translation, and alternative splicing.

### 3.2.3 Coregulated transcripts and proteins in IAV-infected DTC

Next, we aimed to identify a reliable core set of IAV-induced gene expression changes coinciding with the transcript and protein

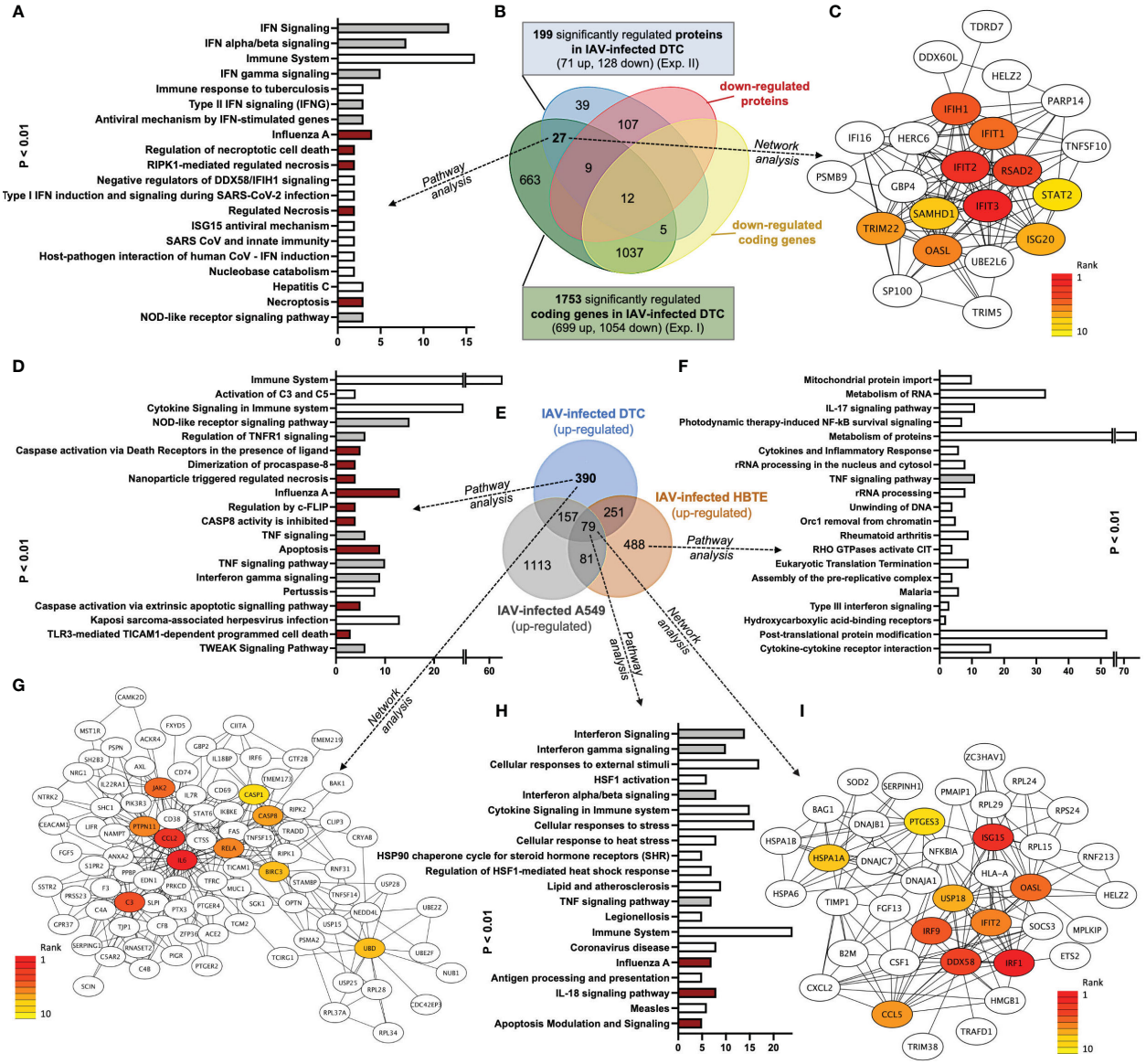


FIGURE 5
Venn, Network, and GO pathway analyses of common upregulated transcripts and proteins after IAV infection of DTC and upregulated transcripts of IAV-infected DTC, A549, and HBTE cells (dark red depicts pathways directly implicated in PANoptosis; grey shows PANoptosis assisting pathways). **(A)** Pathway analysis of 27 shared upregulated genes (*y*-axis sorted by *p*-value, lowest on top; the *x*-axis shows the count of elements in each pathway). **(B)** Venn analysis of regulated genes in transcriptome and proteome in DTC, separated by up- and downregulation. More proteins (128) and protein-coding transcripts (1,753) are downregulated after IAV infection. **(C)** Core interactions of 27 shared upregulated genes (network/centrality analysis; red represents the highest centrality score). **(D)** Pathway analysis of 390 genes only upregulated in DTC (*y*-axis sorted by *p*-value, lowest on top; the *x*-axis shows the count of elements in each pathway). **(E)** Venn analysis of upregulated genes in DTC, HBTE, and A549 cells 12 h after IAV infection. **(F)** Pathway analysis of 488 genes only upregulated in HBTE (*y*-axis sorted by *p*-value, lowest on top; the *x*-axis shows the count of elements in each pathway). **(G)** Core interactions of proteins coded by 390 only upregulated transcripts in DTC (network/centrality analysis; red represents the highest centrality score). **(H)** Pathway analysis of 79 shared upregulated genes in DTC, HBTE, and A549 cells (*y*-axis sorted by *p*-value, lowest on top; the *x*-axis shows the count of elements in each pathway). **(I)** Core interactions of proteins coded by 79 shared upregulated genes in DTC, HBTE, and A549 cells (network/centrality analysis; red represents the highest centrality score).

level in IAV-infected DTC at a late stage of infection (12 hpi). Pathway analysis of 27 mutually upregulated genes and their correlated proteins (Figures 5A, B; Supplementary Table S4) exposed, especially interferon signaling, members of the IAV infection-related KEGG pattern, regulation of and necroptotic cell death (mixed lineage kinase domain-like pseudokinase (MLKL) as well as TNFSF10 (TRAIL), and ISG15 antiviral mechanism to be significantly over-represented (Figure 5A; Supplementary Table S4). Furthermore, network analysis highlighted factors of the antiviral defense as core nodes, including interferon response genes like IFIH1, IFIT3, RSAD2, IRF9, OASL, and IFIT1/2 (Figure 5C). The shared set of combined downregulated transcripts and proteins (12) analyzed by pathway analysis (Supplementary Table S4) pointed out neovascularization processes and Notch signaling. In addition, the shared set of downregulated transcripts and proteins investigated by GO

analysis highlights mesenchymal cell differentiation and kidney epithelium development, among others (Supplementary Table S4). In conclusion, pathway analysis of coregulated transcripts and proteins revealed induction of especially interferon responses and necroptotic cell death, as well as a downregulation of kidney epithelium development, among others.

### 3.3 Comparison of transcriptomic data from H1N1 IAV-infected DTC, A549, and HBTE cells highlights activation of necroptosis, pyroptosis, and apoptosis

In order to identify a pathology-related gene set dominant in IAV-infected DTC, a comparison with available gene expression omnibus (GEO) data from H1N1-type IAV-infected human A549 alveolar and primary HBTE cells (Heinz et al., 2018; Zhao et al., 2018) was performed (Figures 5D–F; Supplementary Table S5). Here, we identified 79 shared upregulated (Figures 5E, H, I; Supplementary Table S6) and 134 shared downregulated genes across all three H1N1 IAV-infected cell lines (Supplementary Table S6). Furthermore, the analysis of genes only upregulated in infected DTC revealed members of highly specific pathways (Figure 5D; Supplementary Table S7), such as activation of complement C3 and C5, the NOD-like receptor (NLR) signaling pathway, regulation of TNFR1 signaling, caspase activation via death receptors, and several pathways involved in regulated cell death, among others (Figure 5D; Supplementary Table S7). In addition, network analysis of genes only upregulated in infected DTC centered factors important in apoptosis, inflammation, the complement system, and ubiquitination (Figure 5G). Furthermore, gasdermin B (GSDMB) and caspase-1 (CASP1), which represent essential factors in pyroptosis (Chen et al., 2018; Tsuchiya et al., 2019; Feng et al., 2022), were upregulated only in infected DTC (Supplementary Table S6). However, evidence for regulated cell death was also present in primary human HBTE and A549 cells (Figures 5E, H; Supplementary Table S6). Although no regulated cell death pathways were among the top 20 pathways (Figure 5F), IL-17 signaling was enriched in HBTE cells compared to DTC and A549 cells (Figure 5F). Notably, the infection-induced proteotoxic stress response was also among the highly enriched pathways in upregulated genes from IAV-infected DTC, HBTE-, and A549 cells (Figure 5H), while network analysis reiterated the ISG15 antiviral response (Figure 5I). Crucially, up-regulation of necroptosis and pyroptosis-associated proteins such as MLKL, TNSF10, IRF9, STAT2, and GBP4 were also identified in the proteome analysis of IAV-infected DTC (Figure 5B; Supplementary Figure S3; Supplementary Tables S2, S3). For the downregulated gene set in DTC, pathway analysis identified regulation of androgen receptor activity, ephrin signaling, and the RHO GTPase cycle, among others (Supplementary Table S7). Taken together, a significant inflammatory response (CCL2, IL6, RELA, JAK2), along with factors of pathogen detection (NLR pathway), upregulation of complement (C3, C5), as well as necroptosis, pyroptosis, and apoptosis indicated by transcripts of pore-forming proteins (MLKL, GSDMD, GSDMB, among others) and caspases (Figure 5E; Supplementary Figures S3, S4; Supplementary Tables S6, S7) are prominent features of IAV-infected primary DTC.

### 3.4 Inhibition of regulated cell death decreases viral-induced cytopathic effects and viral titer

Next, the effect of regulated cell death inhibition in $H1N1_{pdm09}$- and $H3N2_{Victoria}$-infected DTC was investigated (Figure 6). To this end, the viral titer as well as the cellular viability with and without emricasan, (EM, a known apoptosis and pyroptosis inhibitor (Natori et al., 2003; Doerflinger et al., 2020)) or/and the necroptosis inhibitor necrosulfonamide (NSA) were studied. The inhibitors alone or in combination had no cytotoxic effect on DTC at the evaluated concentrations (Supplementary Figure S5). Notably, both inhibitors resulted in a significant reduction in viral titer at 24 hpi (Figures 6A, D), while the most substantial effect was achieved by a combined application of EM and NSA in $H1N1_{pdm09}$-infected DTC. In contrast, their effects in $H3N2_{Victoria}$-infected DTC were less pronounced (Figures 6A, D). Furthermore, treatment with EM and NSA preserved cellular integrity, while IAV infection in the absence of the inhibitors resulted in a significant cytopathogenic effect (CPE, Figures 6B, E). Accordingly, cellular ATP levels demonstrated stronger tubular epithelial cell protection by the combination of EM and NSA (Figures 6C, F).

## 4 Discussion

Here, we demonstrate that human IAV as well as human isolates of avian IAV have the capacity to infect (and propagate in) different human kidney cell types. Furthermore, by transcriptome and proteome analyses, we revealed induction of regulated cell death in $H1N1_{pdm09}$-infected primary human DTC, correlating with the observed kidney pathology in autopsies taken from deceased IAV patients. Up to now, IAV-AKI is not entirely understood. Systemic inflammation, shock, and rhabdomyolysis have been proposed to be the main drivers for AKI and ATN in influenza (Joannidis and Forni, 2011; Watanabe, 2013). Yet, several significant observations have been made, for example: (i) the first detailed ATN description in autopsies of influenza victims dating back to 1895 (Kuskow, 1895); (ii) reports on pathologic swelling of tubular kidney epithelia and acute necrosis of especially DTC in human autopsies (Kuskow, 1895; Lucke et al., 1919; Winternitz et al., 1920); (iii) the isolation of infectious IAV from human renal tissue (Kaji et al., 1959) and urine in the twentieth century (Zakstel', 1953; Zhadanov, 1960; Khakpour and Nik-Akhtar, 1977) or, more recently, the detection of viral RNA (by RT-PCR) in urine (Abdulkader et al., 2010; To et al., 2010; Ho et al., 2013) and kidney tissue (Gao et al., 2016) of IAV-infected patients; (iv) the detection of viral antigen (by serum-based immunofluorescence) in necrotic DTC from a large autopsy cohort in 1983 (Zinserling et al., 1983); and (v) the detection of

10.3389/fcimb.2024.1363407

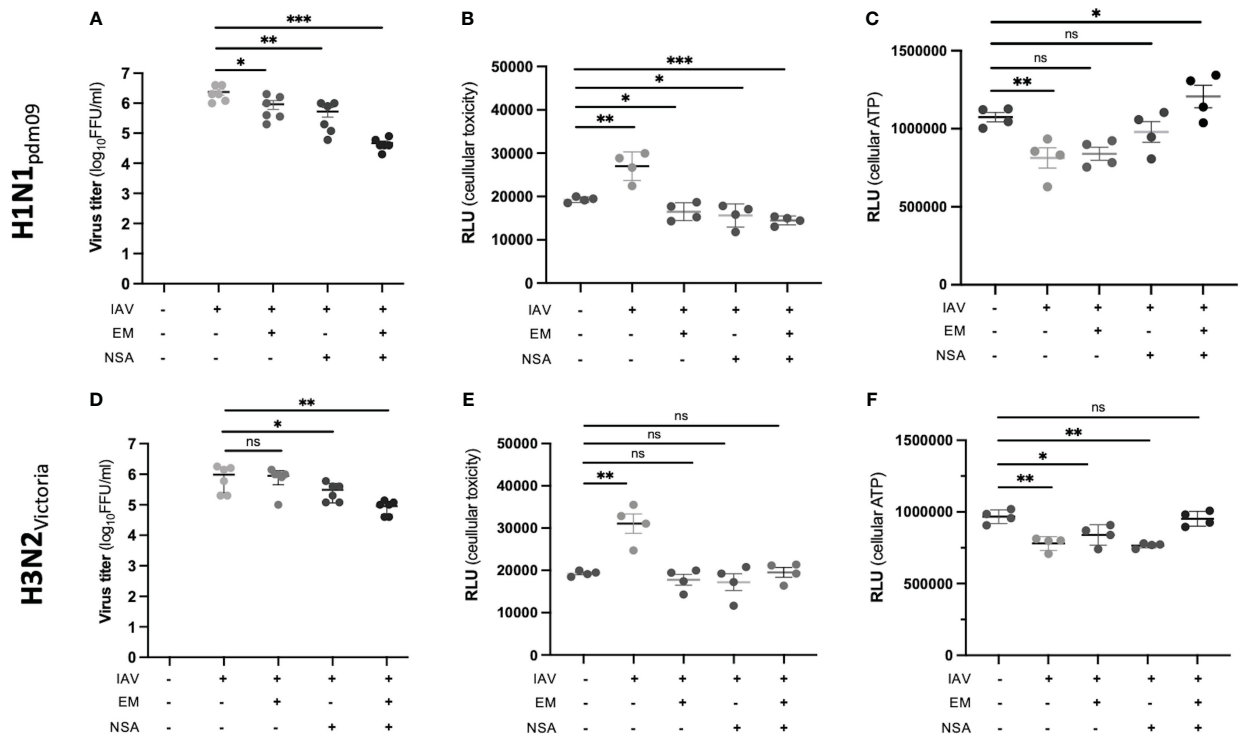


FIGURE 6
Inhibition of IAV replication and IAV-induced epithelial cell toxicity. EM and NSA inhibitors, alone or in combination, were used to assess their ability to inhibit IAV-induced epithelial cell toxicity (each assay: $n = 4$; $*p < 0.05$; $**p < 0.01$; $***p < 0.001$). **(A)** Viral titer of $H1N1_{pdm09}$-infected human DTC at 24 hpi and the effect of inhibitors. **(B)** Analysis of $H1N1_{pdm09}$-induced cytotoxicity and inhibitor effects. The influx of a DNA dye was measured, indicating the membrane integrity's state. **(C)** Analysis of $H1N1_{pdm09}$-induced CPE and inhibitor effects, measured by ATP levels, indicating viable cells. **(D)** Viral titer of $H3N2_{Victoria}$-infected DTC at 24 hpi and the effect of inhibitors. **(E)** Analysis of $H3N2_{Victoria}$-induced cytotoxicity and inhibitor effects. The influx of a DNA dye was measured, indicating the membrane integrity's state. **(F)** Analysis of $H3N2_{Victoria}$-induced CPE and inhibitor effects, measured by ATP levels.

IAV nucleoprotein in DTC (autopsies from 2009) indicative of an ongoing IAV replication in these cells (Nin et al., 2011a). In addition to the tubular lumen, a recent study has demonstrated the susceptibility of DTC to IAV infection from a simulated microcirculation at the basal area (Huangfu et al., 2023). Considering the diameter of IAV (80–120 nm (Noda, 2012) and the renal slit diaphragm width of 20–50 nm (Ruotsalainen et al., 1999), it is therefore plausible that IAV might disseminate to DTC via peritubular capillaries.

In our analyses, all used IAV-infected DTC and PTC demonstrated productive viral replication, while endothelial and glomerular cells displayed strain-dependent results. In IAV-infected DTC transcripts related to necroptosis, apoptosis and pyroptosis were enriched in comparison to the transcriptome of A549 and HBTE cells. Regulated cell death has been identified as a crucial factor in AKI (Linkermann et al., 2014; Miao et al., 2019; Priante et al., 2019) but is also implicated in lung injury in fatal IAV infection (Sauler et al., 2018; Faust and Mangalmurti, 2020). These results, revealing upregulation of factors important in pyroptosis, apoptosis, and necroptosis, could be integrated into the recently proposed model of pyroptosis, apoptosis, and necroptosis (PANoptosis) (Samir et al., 2020; Place et al., 2021). Accordingly, infection or cellular stressors can lead to cell death by the combinatory crosstalk of pyroptotic, apoptotic, and necroptotic molecules (like ZBP1, RIPK1, RIPK3, CASP1, CASP8, and NLRP3, MLKL, and GSMDs) to effectively control pathogenic invasion (Christgen et al., 2020). However, there is also the risk of an excessive inflammatory response, resulting in impaired crucial tissue functions (Balachandran and Rall, 2020). Therefore, we investigated the effects of regulated cell death inhibition in IAV-infected DTC by the pan-caspase inhibitor EM (Hoglen et al., 2004) and the necroptosis inhibitor NSA. The combination of these inhibitors has previously been studied only in IAV-infected monocytes, showing monocyte protection only when used in combination, while effects on epithelial cells or viral titers were not reported (Lee et al., 2019). In our experiments, both EM and NSA resulted in a significant reduction in viral titer at 24 hpi, which was potentiated by the combined application of EM and NSA in $H1N1_{pdm09}$-infected DTC. Importantly, the analysis of tubular viability indicated a preservation of cellular integrity by EM or NSA in H1N1-type and H3N2-type infected DTC.

Regarding the analysis of the downregulated patterns in DTC (shared between transcriptome and proteome), we could detect Notch signaling, while androgen receptor (AR) and Ephrin signaling were enriched for downregulated transcripts in $H1N1_{pdm09}$-infected DTC in comparison to H1N1 IAV-infected

HBTE or A549 cells. Notably, AR signaling limits lung inflammation in an IAV mouse model (Steeg et al., 2020), whereas Ephrin signaling is important for tubular cell cytoarchitecture and survival (Ogawa et al., 2006; Weiss and Kispert, 2016). Moreover, Notch is necessary for the formation of all nephron segments in renal organogenesis (Chung et al., 2017), and alveolar regeneration by epithelial progenitor cells requires Notch to initiate repair (Vaughan et al., 2015). Therefore, it is conceivable that kidney epithelia regeneration is impaired in IAV-infected DTC.

However, this study has limitations. Because we wanted to closely mimic the human environment, the main experiments were done with primary human instead of mouse or canine cells. Thus, we simulated the epithelial aspect of a human tubule, but the effects of pyroptosis/apoptosis inhibition on other cell types than IAV-infected renal cells need to be studied, as other outcomes on virus replication and cellular survival cannot be ruled out. Moreover, as the passage number for primary DTC is limited before they become senescent and the dilution factor is only 1:3, enough primary DTC for either transcriptomic or proteomic analysis could only be gained from two subsequent cell passages. Therefore, we could only relate the shared up- and downregulated transcript and protein levels from two subsequent experiments. Nevertheless, the IAV-induced host-cell shut-off (which is known to target transcription and translation) (Vreede and Fodor, 2010) was reflected in the DTC transcriptome and proteome analysis of these two experiments by the significantly higher number of downregulated transcripts and proteins at 12 hpi. The discrepancy between the number and types of downregulated proteins and the number and types of downregulated transcripts might be explained by posttranslational protein modifications.

In conclusion, IAV can productively replicate on human primary and immortalized nephron cells, and our multiomics analysis of IAV-infected primary human DTC revealed enrichment of multiple programmed cell death pathways (pyroptosis, apoptosis, and necroptosis) with high relevance for IAV- and AKI-related pathology, correlating with the observed kidney pathology in autopsies taken from deceased IAV patients. Consequently, it seems likely that besides classically approved causes like systemic inflammation, shock, and rhabdomyolysis, direct IAV infection of tubular cells can contribute to ATN in IAV-AKI.

## Data availability statement

The datasets presented in this study can be found in online repositories. The names of the repository/repositories and accession number(s) can be found below: https://www.ncbi.nlm.nih.gov/geo/, GSE189735 https://www.ebi.ac.uk/pride/archive, PXD030093.

## Ethics statement

The studies involving humans were approved by Ethics Committee of the Goethe-University Hospital Frankfurt, Germany. The studies were conducted in accordance with the local legislation and institutional requirements. The human samples used in this study were acquired from primarily isolated as part of your previous study for which ethical approval was obtained. Written informed consent for participation was not required from the participants or the participants' legal guardians/next of kin in accordance with the national legislation and institutional requirements.

## Author contributions

BK: Writing – review & editing, Methodology, Writing – original draft, Visualization, Investigation, Funding acquisition, Formal analysis, Conceptualization. MS: Writing – review & editing, Writing – original draft, Visualization, Investigation, Formal analysis. CM-R: Writing – review & editing, Writing – original draft, Investigation, Formal analysis. SG: Writing – review & editing, Visualization, Writing – original draft, Investigation, Formal analysis. NW: Writing – review & editing, Writing – original draft. SP: Writing – review & editing, Writing – original draft. AS: Writing – review & editing, Formal analysis, Writing – original draft. TS: Writing – review & editing, Writing – original draft, Resources. UD: Writing – review & editing, Writing – original draft, Conceptualization. CM: Writing – review & editing, Writing – original draft, Resources, Formal analysis. JZ: Resources, Writing – review & editing, Writing – original draft. HG: Writing – review & editing, Writing – original draft, Resources. LM-S: Writing – review & editing, Writing – original draft. PB: Writing – review & editing, Writing – original draft, Resources. AM: Writing – review & editing, Writing – original draft, Visualization, Investigation, Funding acquisition, Formal analysis. StP: Writing – review & editing, Writing – original draft, Supervision, Resources, Funding acquisition, Conceptualization.

## Funding

The author(s) declare that financial support was received for the research, authorship, and/or publication of this article. The research was funded in part by the University Hospital Frankfurt am Main, a postdoctoral fellowship of the Justus-Liebig University, Giessen, Germany (Just'Us to AM), and the NRC internal project (TT110801 to AM). Furthermore, the Deutsche Forschungsgemeinschaft (DFG, German Research Foundation) funded collaborative research center SFB1021 (TP C01 to StP) and the German Ministry for Education and Research (BMBF) funded German Center for Infection Research, partner site Giessen, Germany (DZIF, TTU 01.806 to SP and JZ). The research was also funded by the Alexander von Humboldt Foundation with a Georg Forster Research Fellowship (MS). StP is a member of the German FluResearchNet, a nationwide research network on zoonotic influenza. Research on influenza in the LM-S laboratory is partially supported by the R01AI145332 and R01AI141607 grants from the National Institute of Health (NIH); by the Center for Research on Influenza Pathogenesis and Transmission (CRIPT), one of the National Institute of Allergy and Infectious Diseases (NIAID)-funded Centers of Excellence for Influenza Research and Response (CEIRR; contract No.

75N93021C00014); and by the American Lung Association. The funders had no role in study design, data collection/analysis, decision to publish, or preparation of the manuscript.

The author(s) declared that they were an editorial board member of Frontiers, at the time of submission. This had no impact on the peer review process and the final decision.

## Acknowledgments

The authors gratefully acknowledge Rita Schmitt-Prokopp and Michael Lein (Department of Urology, Sana Hospital, Offenbach, Germany) for providing us with human renal tissue. Also, Simon C. Satchell and Moin A. Saleem (Bristol Renal, Bristol, UK) are gratefully acknowledged for providing immortalized cell lines.

## Conflict of interest

The authors declare that the research was conducted in the absence of any commercial or financial relationships that could be construed as a potential conflict of interest.

## Publisher's note



## Supplementary material

The Supplementary Material for this article can be found online at: https://www.frontiersin.org/articles/10.3389/fcimb.2024.1363407/full#supplementary-material

## References

Abdulkader, R. C. R. M., Ho, Y. L., Santos, S., de, S., Caires, R., Arantes, M. F., et al. (2010). Characteristics of acute kidney injury in patients infected with the 2009 influenza A (H1N1) virus. *CJASN* 5, 1916–1921. doi: 10.2215/CJN.00840110

Baer, P. C., Nockher, W. A., Haase, W., and Scherberich, J. E. (1997). Isolation of proximal and distal tubule cells from human kidney by immunomagnetic separation: Technical Note. *Kidney Int.* 52, 1321–1331. doi: 10.1038/ki.1997.457

Balachandran, S., and Rall, G. F. (2020). Benefits and perils of necroptosis in influenza virus infection. *J. Virol.* 94, e01101–19. doi: 10.1128/JVI.01101-19

Bercovich-Kinori, A., Tai, J., Gelbart, I. A., Shitrit, A., Ben-Moshe, S., Drori, Y., et al. (2016). A systematic view on influenza induced host shutoff. *eLife* 5, 600. doi: 10.7554/eLife.18311.021

Beswick, I. P., and Finlayson, R. (1959). A renal lesion in association with Influenza. *J. Clin. Pathol.* 12, 280. doi: 10.1136/jcp.12.3.280

Bolger, A. M., Lohse, M., and Usadel, B. (2014). Trimmomatic: a flexible trimmer for Illumina sequence data. *Bioinformatics* 30, 2114–2120. doi: 10.1093/bioinformatics/btu170

Bray, N. L., Pimentel, H., Melsted, P., and Pachter, L. (2016). Near-optimal probabilistic RNA-seq quantification. *Nat. Biotechnol.* 34, 525–527. doi: 10.1038/nbt.3519

Chen, Q., Shi, P., Wang, Y., Zou, D., Wu, X., Wang, D., et al. (2018). GSDMB promotes non-canonical pyroptosis by enhancing caspase-4 activity. *J. Mol. Cell Biol.* 11, 496–508. doi: 10.1093/jmcb/mjy056

Chin, C.-H., Chen, S.-H., Wu, H.-H., Ho, C.-W., Ko, M.-T., and Lin, C.-Y. (2014). cytoHubba: identifying hub objects and sub-networks from complex interactome. *BMC Syst. Biol.* 8, S11. doi: 10.1186/1752-0509-8-S4-S11

Christgen, S., Zheng, M., Kesavardhana, S., Karki, R., Malireddi, R. K. S., Banoth, B., et al. (2020). Identification of the PANoptosome: A molecular platform triggering pyroptosis, apoptosis, and necroptosis (PANoptosis). *Front. Cell Infect. Mi* 10. doi: 10.3389/fcimb.2020.00237

Chung, E., Deacon, P., and Park, J.-S. (2017). Notch is required for the formation of all nephron segments and primes nephron progenitors for differentiation. *Development* 144, 4530–4539. doi: 10.1242/dev.156661

Doerflinger, M., Deng, Y., Whitney, P., Salvamoser, R., Engel, S., Kueh, A. J., et al. (2020). Flexible usage and interconnectivity of diverse cell death pathways protect against intracellular infection. *Immunity* 53, 533–547.e7. doi: 10.1016/j.immuni.2020.07.004

Ersoy, E. O., Er, B., Ciftci, F., Gulleroglu, A., Suner, K., Arpinar, B., et al. (2021). Outcome of patients admitted to intensive care units due to influenza-related severe acute respiratory illness in 2017–2018 flu season: A multicenter study from Turkey. *Respiration* 99, 954–960. doi: 10.1159/000511092

Faust, H., and Mangalmurti, N. S. (2020). Collateral damage: necroptosis in the development of lung injury. *Am. J. Physiol-lung C* 318, L215–L225. doi: 10.1152/ajplung.00065.2019

Feng, H.-H., Zhu, Z.-X., Cao, W.-J., Yang, F., Zhang, X.-L., Du, X.-L., et al. (2018). Foot-and-mouth disease virus induces lysosomal degradation of NME1 to impair p53-regulated interferon-inducible antiviral genes expression. *Cell Death Dis.* 9, 885. doi: 10.1038/s41419-018-0940-z

Feng, Y., Li, M., Yangzhong, X., Zhang, X., Zu, A., Hou, Y., et al. (2022). Pyroptosis in inflammation-related respiratory disease. *J. Physiol. Biochem.* 78, 721–737. doi: 10.1007/s13105-022-00909-1

Gamboa, E. T., Eastwood, A. B., Hays, A. P., Maxwell, J., and Penn, A. S. (1979). Isolation of influenza virus from muscle in myoglobinuric polymyositis. *Neurology* 29, 1323–1335. doi: 10.1212/WNL.29.10.1323

Gao, R., Pan, M., Li, X., Zou, X., Zhao, X., Li, T., et al. (2016). Post-mortem findings in a patient with avian influenza A (H5N6) virus infection. *Clin. Microbiol. Infection* 22, 574.e1–574.e5. doi: 10.1016/j.cmi.2016.03.017

Ge, S. X., Jung, D., and Yao, R. (2019). ShinyGO: a graphical gene-set enrichment tool for animals and plants. *Bioinformatics* 36, 2628–2629. doi: 10.1093/bioinformatics/btz931

Ge, S. X., Son, E. W., and Yao, R. (2018). iDEP: an integrated web application for differential expression and pathway analysis of RNA-Seq data. *BMC Bioinf.* 19, 534. doi: 10.1186/s12859-018-2486-6

Heinz, S., Texari, L., Hayes, M. G. B., Urbanowski, M., Chang, M. W., Givarkes, N., et al. (2018). Transcription elongation can affect genome 3D structure. *Cell* 174, 1522–1536.e22. doi: 10.1016/j.cell.2018.07.047

Ho, Y.-L., Yoshino, A., Tonacio, A. C., Latif, A. Z. A., Filho, H. H. C., and dos Santos, S. D. S. (2013). Detection of pandemic influenza-A(H1N1)-2009 virus in urine. *Intensiv. Care Med.* 39, 1168–1169. doi: 10.1007/s00134-013-2921-0

Hoglen, N. C., Chen, L.-S., Fisher, C. D., Hirakawa, B. P., Groessl, T., and Contreras, P. C. (2004). Characterization of IDN-6556 (3-{2-(2-tert-butyl-phenylaminooxalyl)-amino]-propionylamino}-4-oxo-5-(2,3,5,6-tetrafluoro-phenoxy)-pentanoic acid): a liver-targeted caspase inhibitor. *J. Pharmacol. Exp. Ther.* 309, 634–640. doi: 10.1124/jpet.103.062034

Hsu, C.-H., Chen, H.-P., Chen, P.-L., and Chan, Y.-J. (2022). Detection of influenza and non-influenza respiratory viruses in lower respiratory tract specimens among hospitalized adult patients and analysis of the clinical outcome. *J. Microbiol. Immunol. Infect.* 55, 820–828. doi: 10.1016/j.jmii.2021.12.001

Huangfu, Y., Wang, J., Feng, J., and Zhang, Z.-L. (2023). Distal renal tubular system-on-a-chip for studying the pathogenesis of influenza A virus-induced kidney injury. *Lab. Chip* 23, 4255–4264. doi: 10.1039/D3LC00616F

Ibricevic, A., Pekosz, A., Walter, M. J., Newby, C., Battaile, J. T., Brown, E. G., et al. (2006). Influenza virus receptor specificity and cell tropism in mouse and human airway epithelial cells. *J. Virol.* 80, 7469–7480. doi: 10.1128/JVI.02677-05

Iuliano, A. D., Roguski, K. M., Chang, H. H., Muscatello, D. J., Palekar, R., Tempia, S., et al. (2018). Estimates of global seasonal influenza-associated respiratory mortality: a modelling study. *Lancet* 391, 1285–1300. doi: 10.1016/S0140-6736(17)33293-2

Jamoussi, A., Ayed, S., Merhabene, T., Doghri, H., Khelil, J. B., and Besbes, M. (2022). Severe influenza A in a Tunisian ICU sentinel SARI centre: Epidemiological and clinical features. *PloS One* 17, e0270814. doi: 10.1371/journal.pone.0270814

Joannidis, M., and Forni, L. G. (2011). Severe viral infection and the kidney: lessons learned from the H1N1 pandemic. *Intensive Care Med.* 37, 729–731. doi: 10.1007/s00134-011-2196-2

Johnson, N. P. A. S., and Mueller, J. (2002). Updating the accounts: global mortality of the 1918-1920 "Spanish" Influenza pandemic. *B Hist Med.* 76, 105–115. doi: 10.1353/bhm.2002.0022

Jong, M. D., de, Simmons, C. P., Thanh, T. T., Hien, V. M., Smith, G. J. D., Chau, T. N. B., et al. (2006). Fatal outcome of human influenza A (H5N1) is associated with high viral load and hypercytokinemia. *Nat. Med.* 12, 1203–1207. doi: 10.1038/nm1477

Kaji, M., Oseasohn, R., Jordan, W. S., and Dingle, J. H. (1959). Isolation of Asian virus from extrapulmonary tissues in fatal human influenza. *Proc. Soc. Exp. Biol. Med.* 100, 272–275. doi: 10.3181/00379727-100-24597

Kamburov, A., Pentchev, K., Galicka, H., Wierling, C., Lehrach, H., and Herwig, R. (2011). ConsensusPathDB: toward a more complete picture of cell biology. *Nucleic Acids Res.* 39, D712–D717. doi: 10.1093/nar/gkq1156

Kanehisa, M. (2000). KEGG: kyoto encyclopedia of genes and genomes. *Nucleic Acids Res.* 28, 27–30. doi: 10.1093/nar/28.1.27

Khakpour, M., and Nik-Akhtar, B. (1977). Epidemics of haemorrhagic cystitis due to influenza A virus. *Postgraduate Med. J.* 53, 251–253. doi: 10.1136/pgmj.53.619.251

Khakpour, M., Saidi, A., and Naficy, K. (1969). Proved viraemia in asian influenza (Hong Kong variant) during incubation period. *BMJ* 4, 208–209. doi: 10.1136/bmj.4.5677.208

Kuskow, N. (1895). Zur pathologischen Anatomie der Grippe. *Archiv Für Pathologische Anatomie Und Physiologie Und Für Klinische Medicin* 139, 406–458. doi: 10.1007/bf01882006

Lee, A. C. Y., Zhang, A. J. X., Chu, H., Li, C., Zhu, H., Mak, W. W. N., et al. (2019). H7N9 influenza A virus activation of necroptosis in human monocytes links innate and adaptive immune responses. *Cell Death Dis.* 10, 198. doi: 10.1038/s41419-019-1684-0

Lee, N., Chan, P. K. S., Lui, G. C. Y., Wong, B. C. K., Sin, W. W. Y., Choi, K.-W., et al. (2011). Complications and outcomes of pandemic 2009 influenza A (H1N1) virus infection in hospitalized adults: how do they differ from those in seasonal influenza? *J. Infect. Dis.* 203, 1739–1747. doi: 10.1093/infdis/jir187

Levene, R. E., and Gaglia, M. M. (2018). Host shutoff in influenza A virus: many means to an end. *Viruses* 10, 475. doi: 10.3390/v10090475

Li, S. (2019). Regulation of ribosomal proteins on viral infection. *Cells* 8, 508. doi: 10.3390/cells8050508

Li, X., Fu, Z., Liang, H., Wang, Y., Qi, X., Ding, M., et al. (2018). H5N1 influenza virus-specific miRNA-like small RNA increases cytokine production and mouse mortality *via* targeting poly(rC)-binding protein 2. *Cell Res.* 28, 157–171. doi: 10.1038/cr.2018.3

Linkermann, A., Chen, G., Dong, G., Kunzendorf, U., Krautwald, S., and Dong, Z. (2014). Regulated cell death in AKI. *JASN* 25, 2689–2701. doi: 10.1681/ASN.2014030262

Lowry, S. A., Wolfe, M. K., and Boehm, A. B. (2023). Respiratory virus concentrations in human excretions that contribute to wastewater: a systematic review and meta-analysis. *J. Water Heal.* 21, 831–848. doi: 10.2166/wh.2023.057

Lucke, B., Wight, T., and Kime, E. (1919). Pathologic anatomy and bacteriology of influenza: epidemic of autumn 1918. *Arch. Intern. Med.* 24, 154–237. doi: 10.1001/archinte.1919.00090250027002

Luo, W., and Brouwer, C. (2013). Pathview: an R/Bioconductor package for pathway-based data integration and visualization. *Bioinformatics* 29, 1830–1831. doi: 10.1093/bioinformatics/btt285

Ma, W., Brenner, D., Wang, Z., Dauber, B., Ehrhardt, C., Högner, K., et al. (2009). The NS segment of an H5N1 highly pathogenic avian influenza virus (HPAIV) is sufficient to alter replication efficiency, cell tropism, and host range of an H7N1 HPAIV. *J. Virol.* 84, 2122–2133. doi: 10.1128/JVI.01668-09

Martin-Loeches, I., Papiol, E., Rodríguez, A., Diaz, E., Zaragoza, R., Granada, R. M., et al. (2011). Acute kidney injury in critical ill patients affected by influenza A (H1N1) virus infection. *Crit. Care* 15, R66. doi: 10.1186/cc10046

Matias, G., Haguinet, F., Lustig, R. L., Edelman, L., Chowell, G., and Taylor, R. J. (2016). Model estimates of the burden of outpatient visits attributable to influenza in the United States. *BMC Infect. Dis.* 16, 641. doi: 10.1186/s12879-016-1939-7

Mering, C., von, Huynen, M., Jaeggi, D., Schmidt, S., Bork, P., and Snel, B. (2003). STRING: a database of predicted functional associations between proteins. *Nucleic Acids Res.* 31, 258–261. doi: 10.1093/nar/gkg034

Miao, N., Yin, F., Xie, H., Wang, Y., Xu, Y., Shen, Y., et al. (2019). The cleavage of gasdermin D by caspase-11 promotes tubular epithelial cell pyroptosis and urinary IL-18 excretion in acute kidney injury. *Kidney Int.* 96, 1105–1120. doi: 10.1016/j.kint.2019.04.035

Morens, D. M., and Taubenberger, J. K. (2018). The mother of all pandemics is 100 years old (and going strong)! *Am. J. Public Health* 108, 1449–1454. doi: 10.2105/ajph.2018.304631

Mostafa, A., Kanrai, P., Ziebuhr, J., and Pleschka, S. (2013). Improved dual promotor-driven reverse genetics system for influenza viruses. *J. Virol. Methods* 193, 603–610. doi: 10.1016/j.jviromet.2013.07.021

Natori, S., Higuchi, H., Contreras, P., and Gores, G. J. (2003). The caspase inhibitor IDN-6556 prevents caspase activation and apoptosis in sinusoidal endothelial cells during liver preservation injury. *Liver Transplant.* 9, 278–284. doi: 10.1053/jlts.2003.50019

Nin, N., Lorente, J. A., Sánchez-Rodríguez, C., Granados, R., Ver, L. S., Soto, L., et al. (2011b). Kidney histopathological findings in fatal pandemic 2009 influenza A (H1N1). *Intensive Care Med.* 37, 880–881. doi: 10.1007/s00134-011-2183-7

Nin, N., Lorente, J. A., Soto, L., Ríos, F., Hurtado, J., Arancibia, F., et al. (2011a). Acute kidney injury in critically ill patients with 2009 influenza A (H1N1) viral pneumonia: an observational study. *Intensive Care Med.* 37, 768–774. doi: 10.1007/s00134-011-2167-7

Noda, T. (2012). Native morphology of influenza virions. *Front. Microbiol.* 2. doi: 10.3389/fmicb.2011.00269

Ogawa, K., Wada, H., Okada, N., Harada, I., Nakajima, T., Pasquale, E. B., et al. (2006). EphB2 and ephrin-B1 expressed in the adult kidney regulate the cytoarchitecture of medullary tubule cells through Rho family GTPases. *J. Cell Sci.* 119, 559–570. doi: 10.1242/jcs.02777

Pfaffl, M. W. (2001). A new mathematical model for relative quantification in real-time RT-PCR. *Nucleic Acids Res.* 29, e45–e45. doi: 10.1093/nar/29.9.e45

Pico, A. R., Kelder, T., Iersel, M. P., Hanspers, K., Conklin, B. R., and Evelo, C. (2008). WikiPathways: pathway editing for the people. *PloS Biol.* 6, e184. doi: 10.1371/journal.pbio.0060184

Pimentel, H., Bray, N. L., Puente, S., Melsted, P., and Pachter, L. (2017). Differential analysis of RNA-seq incorporating quantification uncertainty. *Nat. Methods.* 14, 687–690. doi: 10.1038/nmeth.4324

Place, D. E., Lee, S., and Kanneganti, T.-D. (2021). PANoptosis in microbial infection. *Curr. Opin. Microbiol.* 59, 42–49. doi: 10.1016/j.mib.2020.07.012

Pleschka, S., Kanrai, P., Ziebuhr, J., and Mostafa, A. (2016). The PB1 segment of an influenza A virus H1N1 2009pdm isolate enhances the replication efficiency of specific influenza vaccine strains in cell culture and embryonated eggs. *J. Gen. Virol.* 97, 620–631. doi: 10.1099/jgv.0.000390

Priante, G., Gianesello, L., Ceol, M., Prete, D. D., and Anglani, F. (2019). Cell death in the kidney. *Int. J. Mol. Sci.* 20, 3598. doi: 10.3390/ijms20143598

Rolfes, M. A., Foppa, I. M., Garg, S., Flannery, B., Brammer, L., Singleton, J. A., et al. (2018). Annual estimates of the burden of seasonal influenza in the United States: A tool for strengthening influenza surveillance and preparedness. *Influenza Other Resp.* 12, 132–137. doi: 10.1111/irv.12486

Ruotsalainen, V., Ljungberg, P., Wartiovaara, J., Lenkkeri, U., Kestilä, M., Jalanko, H., et al. (1999). Nephrin is specifically located at the slit diaphragm of glomerular podocytes. *Proc. Natl. Acad. Sci.* 96, 7962–7967. doi: 10.1073/pnas.96.14.7962

Saleem, M. A., O'Hare, M. J., Reiser, J., Coward, R. J., Inward, C. D., Farren, T., et al. (2002). A conditionally immortalized human podocyte cell line demonstrating nephrin and podocin expression. *JASN* 13, 630–638. doi: 10.1681/ASN.V133630

Samir, P., Malireddi, R. K. S., and Kanneganti, T.-D. (2020). The PANoptosome: A deadly protein complex driving pyroptosis, apoptosis, and necroptosis (PANoptosis). *Front. Cell Infect. Mi* 10. doi: 10.3389/fcimb.2020.00238

Sarrab, R. M., Lennon, R., Ni, L., Wherlock, M. D., Welsh, G. I., and Saleem, M. A. (2011). Establishment of conditionally immortalized human glomerular mesangial cells in culture, with unique migratory properties. *Am. J. Physiol.* 301, F1131–F1138. doi: 10.1152/ajprenal.00589.2010

Satchell, S. C., Tasman, C. H., Singh, A., Ni, L., Geelen, J., von Ruhland, C. J., et al. (2006). Conditionally immortalized human glomerular endothelial cells expressing fenestrations in response to VEGF. *Kidney Int.* 69, 1633–1640. doi: 10.1038/sj.ki.5000277

Sauler, M., Bazan, I. S., and Lee, P. J. (2018). Cell death in the lung: the apoptosis–necroptosis axis. *Annu. Rev. Physiol.* 81, 1–28. doi: 10.1146/annurev-physiol-020518-114320

Shannon, P., Markiel, A., Ozier, O., Baliga, N. S., Wang, J. T., Ramage, D., et al. (2003). Cytoscape: A software environment for integrated models of biomolecular interaction networks. *Genome Res.* 13, 2498–2504. doi: 10.1101/gr.1239303

Short, K. R., Kroeze, E. J. B. V., Fouchier, R. A. M., and Kuiken, T. (2014). Pathogenesis of influenza-induced acute respiratory distress syndrome. *Lancet Infect. Dis.* 14, 57–69. doi: 10.1016/S1473-3099(13)70286-X

Siefkes, H., Hamele, M., Ampofo, K., and Poss, W. (2015). Risk factors for poor outcomes and therapeutic strategies for seasonal and pandemic influenza. *J. Pediatr. Intensive Care* 03, 217–226. doi: 10.3233/PIC-14104

Steeg, L. G., vom, Dhakal, S., Woletsadik, Y. A., Park, H.-S., Mulka, K. R., Reilly, E. C., et al. (2020). Androgen receptor signaling in the lungs mitigates inflammation and improves the outcome of influenza in mice. *PloS Pathog.* 16, e1008506. doi: 10.1371/journal.ppat.1008506

Taubenberger, J. K., and Morens, D. M. (2006). 1918 Influenza: the mother of all pandemics. *Emerging Infect. Dis.* 12, 15–22. doi: 10.3201/eid1209.05-0979

Thakkar, J., and Golestaneh, L. (2021). The changing epidemiology of acute kidney injury syndromes in the face of emerging respiratory viral pandemic illnesses. *Kidney Int.* 100, 750–752. doi: 10.1016/j.kint.2021.07.001

To, K. K. W., Chan, K.-H., Li, I. W. S., Tsang, T.-Y., Tse, H., Chan, J. F. W., et al. (2010). Viral load in patients infected with pandemic H1N1 2009 influenza A virus. *J. Med. Virol.* 82, 1–7. doi: 10.1002/jmv.21664

Tse, H., To, K. K. W., Wen, X., Chen, H., Chan, K.-H., Tsoi, H.-W., et al. (2011). Clinical and virological factors associated with viremia in pandemic influenza A/H1N1/2009 virus infection. *PloS One* 6, e22534. doi: 10.1371/journal.pone.0022534

Tsuchiya, K., Nakajima, S., Hosojima, S., Nguyen, D. T., Hattori, T., Le, T. M., et al. (2019). Caspase-1 initiates apoptosis in the absence of gasdermin D. *Nat. Commun.* 10, 2091. doi: 10.1038/s41467-019-09753-2

Ulloa, F., and Real, F. X. (2001). Differential distribution of sialic acid in alpha2,3 and alpha2,6 linkages in the apical membrane of cultured epithelial cells and tissues. *J. Histochem. Cytochem.* 49, 501–510. doi: 10.1177/002215540104900410

Vastrik, I., D'Eustachio, P., Schmidt, E., Joshi-Tope, G., Gopinath, G., Croft, D., et al. (2007). Reactome: a knowledge base of biologic pathways and processes. *Genome Biol.* 8, R39. doi: 10.1186/gb-2007-8-3-r39

Vaughan, A. E., Brumwell, A. N., Xi, Y., Gotts, J. E., Brownfield, D. G., Treutlein, B., et al. (2015). Lineage-negative progenitors mobilize to regenerate lung epithelium after major injury. *Nature* 517, 621–625. doi: 10.1038/nature14112

Vreede, F. T., and Fodor, E. (2010). The role of the influenza virus RNA polymerase in host shut-off. *Virulence* 1, 436–439. doi: 10.4161/viru.1.5.12967

Watanabe, T. (2013). Renal complications of seasonal and pandemic influenza A virus infections. *Eur. J. Pediatr.* 172, 15–22. doi: 10.1007/s00431-012-1854-x

Weiss, A.-C., and Kispert, A. (2016). Eph/ephrin signaling in the kidney and lower urinary tract. *Pediatr. Nephrol.* 31, 359–371. doi: 10.1007/s00467-015-3112-8

Winternitz, M. C., McNamara, F. P., and Wason, I. M. (1920). *The Pathology of Influenza*. New Haven, CI, USA: Yale University Press.

Yao, L., Korteweg, C., Hsueh, W., and Gu, J. (2008). Avian influenza receptor expression in H5N1-infected and noninfected human tissues. *FASEB J.* 22, 733–740. doi: 10.1096/fj.06-7880com

Yawn, D. H., Pyeatte, J. C., Joseph, J. M., Eichler, S. L., and Garcia-Bunuel, R. (1971). Transplacental transfer of influenza virus. *JAMA* 216, 1022–1023. doi: 10.1001/jama.1971.03180320064016

Zakstel'skaya. (1953). *Recovery of virus from urine of patients with epidemic influenza. OKVDP Tr ob'yed sess AMN SSSR*, 72–4.

Zhadanov, V. M. (1960). "The Study of Influenza," in *A translation of ucheniye o grippe (Moscow, Medgiz, 1958)*. Bethesda, Maryland, USA, National Institutes of Health.

Zhao, N., Sebastiano, V., Moshkina, N., Mena, N., Hultquist, J., Jimenez-Morales, D., et al. (2018). Influenza virus infection causes global RNAPII termination defects. *Nat. Struct. Mol. Biol.* 25, 885–893. doi: 10.1038/s41594-018-0124-7

Zinserling, V. A., Aksenov, O. A., Melnikova, V. F., and Zinserling, V. A. (1983). Extrapulmonary lesions in influenza. *Tohoku J. Exp. Med.* 140, 259–272. doi: 10.1620/tjem.140.259